Advances in Engineering Research : Possibilities and Challenges
ISSN Print: 3079-5192
ISSN Online: 3079-5206
https://doi.org/10.63313/AERpc.9019

Effect of Fiber Orientation on Grinding Characteristics and Removal Mechanisms of C_f/SiC

Runxian Luo*. Ruizhi Hu
School of Mechanical and Power Engineering, Henan Polytechnic University, Jiaozuo 454003, China.
Email: 540340812@qq.com

How to cite this paper: Luo, R. X., & Hu, R. Z. (2025). Effect of Fiber Orientation on Grinding Characteristics and Removal Mechanisms of C_f/SiC. Advances in Engineering Research : Possibilities and Challenges, 1(2), 51-60. ISSN Print: 3079-5192; ISSN Online: 3079-5206.
https://doi.org/10.63313/AERpc.9019
Published: 2025-05-06

Abstract

Carbon fiber-reinforced silicon carbide ceramic matrix composites (Cf/SiC) ex-hibit advantages such as high-temperature resistance, low density, and high spe-cific strength, making them widely applicable in aerospace, new energy vehicles, and other fields. However, their heterogeneous nature and hard-brittle fracture mechanisms lead to poor machined surface quality. To clarify the influence of fiber orientation on grinding characteristics and material removal mechanisms, single-grit scratching experiments were conducted, and a finite element model (FEM) of Cf/SiC composites was established. Two machining directions, MA (transverse direction) and MB (longitudinal direction), were defined based on fiber orientation, and the effects on normal force (Fn) and surface morphology were investigated. A finite element numerical model of Cf/SiC composites was developed, incorporating the mechanical properties of fibers, matrix, and in-ter-faces. Simulation results revealed that Fn increases with cutting depth, and the average Fn magnitude followed the order MB > MA. Cracks propagated along the fiber axis: transverse fibers were removed via wear, fracture, and peeling, with some fibers exposed due to brittle matrix fracture; longitudinal fibers were re-moved via wear and debonding, primarily influenced by the contact area be-tween fibers and abrasive grits.

Keywords

C_f/SiC composites; Single-grit scratching experiment; Finite element analysis

1. Introduction

C_f/SiC composites combine the high hardness, wear resistance, and thermal stability of the silicon carbide matrix [1, 2] with the chemical resistance and low thermal expansion of carbon fibers [3], making them critical for high-performance applications in aerospace, new energy vehicles, and military systems [4, 5]. However, secondary machining is required to meet precision assembly and functional demands [6, 7]. Due to their high hardness, multiphase structure, and anisotropy, machining processes often induce defects such as surface crack propagation, fiber pull-out, and delamination [8, 9]. Grinding has been identified as an effective method to improve surface quality, prompting extensive research into its mechanisms and characteristics.

Zhang et al. [10] investigated the grinding characteristics of Cf/SiC in three orientations and observed that fiber orientation significantly influences material removal, with brittle fiber fracture being the dominant mechanism. Li et al. [11] compared unidirectional and 2.5D woven Cf/SiC composites, finding that fiber arrangement affects fracture modes: fragments parallel to the grinding direction were elongated, while perpendicular fragments were chip-like. Qu et al. [12] studied the effects of fiber orientation and grinding depth on surface morphology, roughness, grinding forces, and chips in 2.5D needle-punched Cf/SiC, concluding that both parameters critically influence surface quality. Cao et al. [13] similarly reported fiber orientation-dependent grinding forces.

Single-grit scratching experiments are effective for studying grinding mechanisms. Liu et al. [14] conducted longitudinal, transverse, and normal scratches on 2D C_f/SiC, observing periodic fluctuations in scratching forces and distinct removal modes dominated by brittle fracture. Wang et al. [15] performed single-diamond grit scratching on C_f/SiC, revealing that parallel scratches caused fiber compression and shear removal, while perpendicular scratches induced crack propagation along fibers with interfacial damage. Lin et al. [16] studied ultrasonic scratching of SiC_f/SiC and found fiber angle-dependent removal mechanisms: shear/bending fracture at 0° and extrusion/debonding at 90°.

Finite element analysis (FEA) offers advantages in visualizing material removal and predicting cutting forces. Zhu et al. [19] developed a 3D macroscopic model for CFRP/Ti laminates using ABAQUS. Du et al. [20] established a multiphase 2D FEA model for SiCp/Al composites to analyze micro-removal mechanisms. Yan et al. [21] modeled fiber, matrix, and interfaces to simulate orthogonal cutting of unidirectional CFRP, providing theoretical guidance for FEA of fiber-reinforced composites. Han et al. [22] combined FEA and experiments to reveal intralayer damage mechanisms in UD-CFRP under nano scratching, linking fiber failure modes to scratching forces. Chen et al. [23] modeled orthogonal cutting of C_f/SiC using maximum stress criteria for fibers and matrix, but oversimplified constitutive models and inaccurate interfacial parameters hinder analysis of damage evolution.

Building on prior work, this study establishes an FEM for single-grit scratching of C_f/SiC, incorporating a brittle matrix constitutive model, orthotropic elastoplastic fiber model, and interfacial properties. Transverse (MA) and longitudinal (MB) scratching experiments were conducted to analyze the effects of depth and fiber orientation on grinding characteristics. The model simulates crack propagation and removal behaviors, elucidating the micro-removal mechanisms under different fiber orientations.

2. Materials and Methods

2.1. Materials

The C_f/SiC composite used in the experiments was fabricated via a combined method of Chemical Vapor Infiltration (CVI) and Precursor Infiltration and Pyrolysis (PIP). It is a carbon fiber-reinforced silicon carbide ceramic matrix composite, composed of carbon fibers and a silicon carbide matrix, as illustrated in Figure 1. The mechanical properties of the material are listed in Table 1.

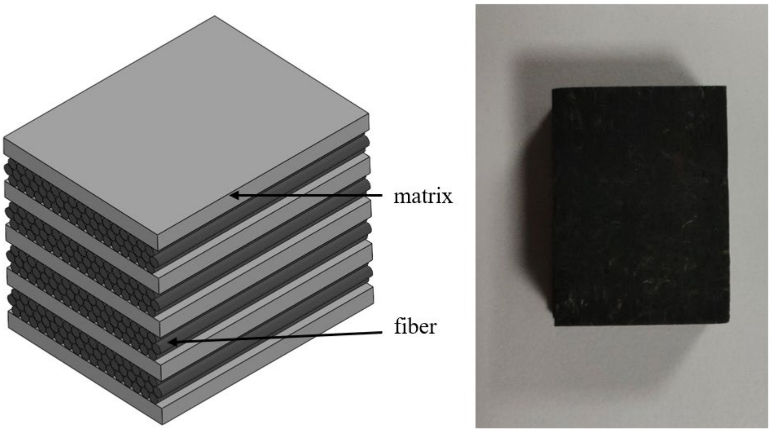

Figure 1. structure diagram and sample diagram of C_f/SiC

Table 1. mechanical properties of C_f/SiC composite

Material	Volume fraction of fiber (%)	Density (g/cm^3)	Bending strength (GPa)	Tensile strength (GPa)	Poisson's ratio
C_f/SiC	30%	1.8	45	70	0.35

2.2. Single-Grit Scratching Experiment

The workpiece dimensions were 20 mm × 15 mm × 10 mm, and a diamond indenter with a 90° conical angle at the tip was used as the tool. A schematic of the experimental setup is shown in Figure 2. Based on fiber orientation, two machining directions were designed: MA (transverse direction) and MB (longitudinal direction). Experiments were conducted at varying scratching depths (ap), with three repetitions per depth. The experimental parameters were set as follows: feed speed V=100 mm/min, and scratching depths ap = 3, 6, and 9 μm.

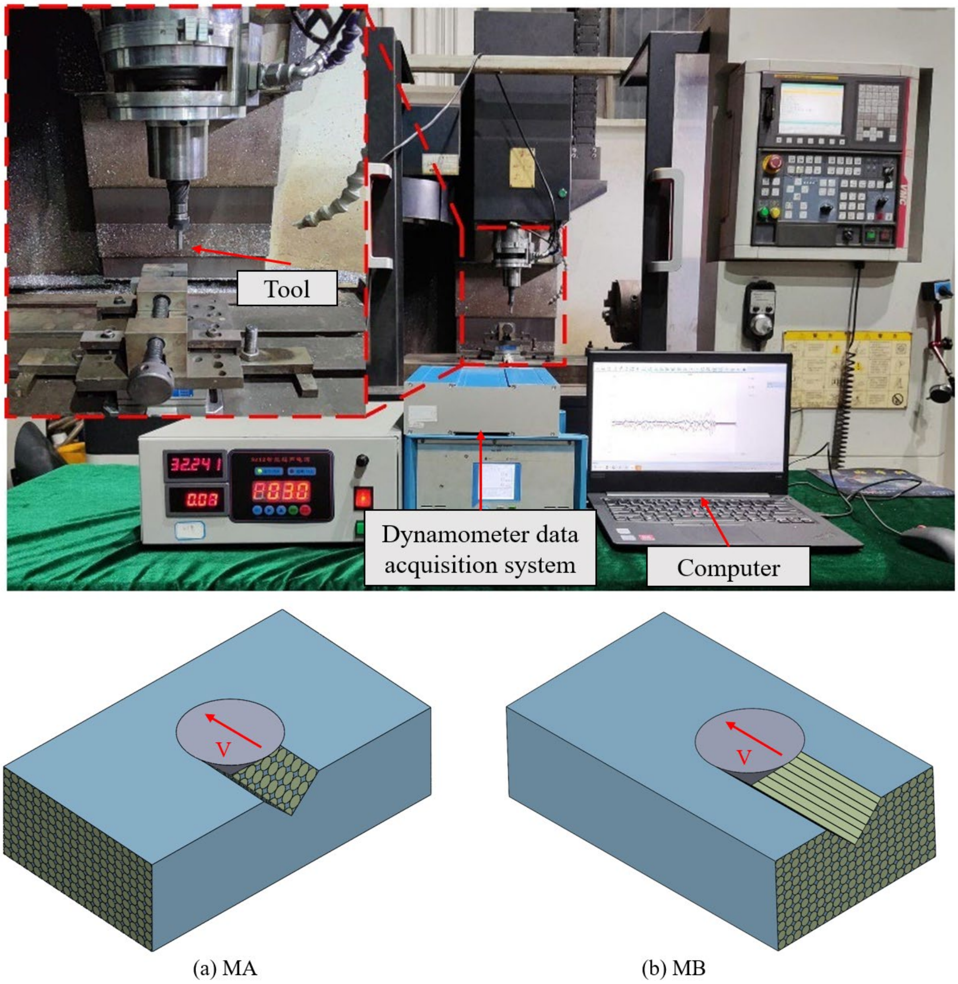

Figure 2. Experimental site and processing direction diagram

2.3. Single-Grit Scratching Simulation

To visualize the material removal process and elucidate the effects of cutting forces and surface morphology, a finite element numerical model for single-grit grinding of C_f/SiC composites was established using Abaqus software. This model comprehensively accounts for matrix brittleness, fiber anisotropy, and interfacial mechanical properties, exploring the grinding mechanisms of C_f/SiC composites and providing critical theoretical insights for production.

2.4. Geometric Model

Based on the actual composition of C_f/SiC composites, a finite element simulation model was developed, considering fiber arrangement and mechanical properties. The geometric dimensions of the model were 100 μm × 50 μm × 25 μm, with a fiber diameter d=7 μm. By adjusting the grit position, scratching at different angles was simulated. Due to computational limitations in replicating the dense and complex fiber distribution of real materials, the model focused on single or multiple fibers rather than full-scale simulations. To align with the model's scale, the feed speed V was set to 10 m/s, and scratching depths ap were 5, 8, and 10 μm. These parameters enabled the study of semi-cutting, full-cutting, and complete cutting of individual or multiple fibers, thereby analyzing crack propagation and failure modes.

As shown in Figure 3, the abrasive grit was simplified to a 90° conical indenter without fillets and modeled as a discrete rigid body [24]. The workpiece's bottom face was fully constrained, and displacements on both sides along the scratching direction were restricted. A penalty contact algorithm was applied between the grit, fibers, and matrix to enforce interfacial constraints. The friction coefficients were defined as follows: 0.35 between the grit and matrix [25], 0.8 between the grit and fibers, and 0.8 between fibers and the matrix [26].

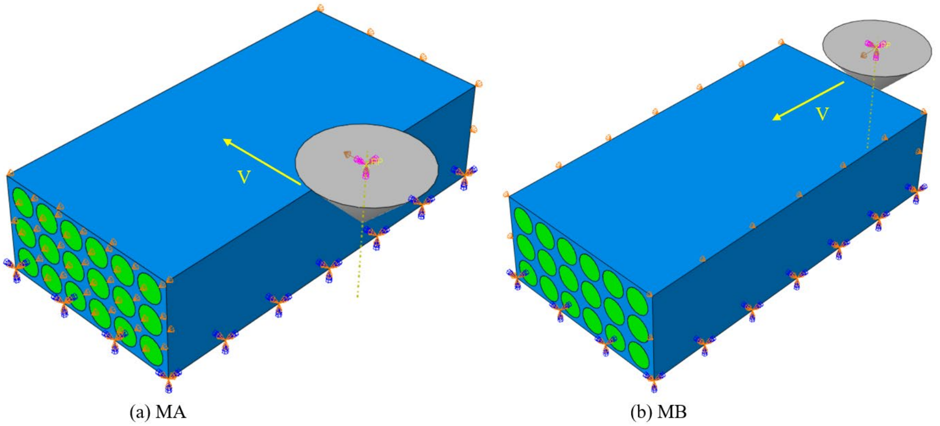

Figure 3. Schematic diagram of model unit and simulation machining directions

3. Results and Analysis

3.1. Scratching Force Analysis

According to indentation fracture mechanics, the normal force (F_n) during scratching effectively reflects machining conditions, making (F_n) a critical evaluation metric. Figure 4 illustrates the simulated (F_n) signal characteristics for the MA direction at a scratching depth of 8 μm. The scratching force exhibits unstable fluctuations with periodic variations, attributed to the periodic arrangement of multiple fibers in the MA direction. The cyclic force behavior comprises two distinct phases: (a) SiC removal and (b) fiber removal.

When the abrasive grit initially contacts the SiC matrix, stress gradually increases until exceeding the ultimate strength of SiC, leading to matrix fracture and removal. As the grit advances, weaker supporting properties of SiC around the fibers cause localized matrix damage, resulting in stress reduction. Upon fiber engagement, the scratching force shows smaller fluctuations. Due to the significantly higher strength of SiC compared to fibers, the scratching force in phase (a) is markedly greater than in phase (b). After fiber removal, the grit recontacts the

SiC matrix, repeating the cycle until scratching completion.

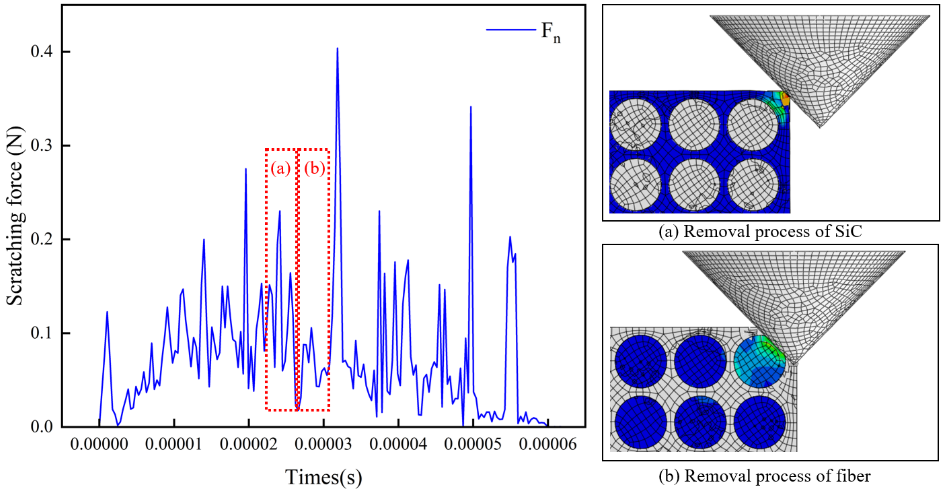

Figure 4. Signal characteristics of scratching force in MA

As shown in Figures 5 and 6, regardless of the scratching angle, both simulations and experiments demonstrate that the normal force (Fn) increases with cutting depth, following the trend MB > MA. This occurs because, at lower cutting depths, the tool interacts with fibers for a longer duration compared to the matrix. Since carbon fibers have a lower Young's modulus than silicon carbide (SiC), this results in a smaller Fn. As the cutting depth increases, the contact area between the tool and material expands, and the volume of material removed per unit time rises with depth, leading to an increase in Fn.

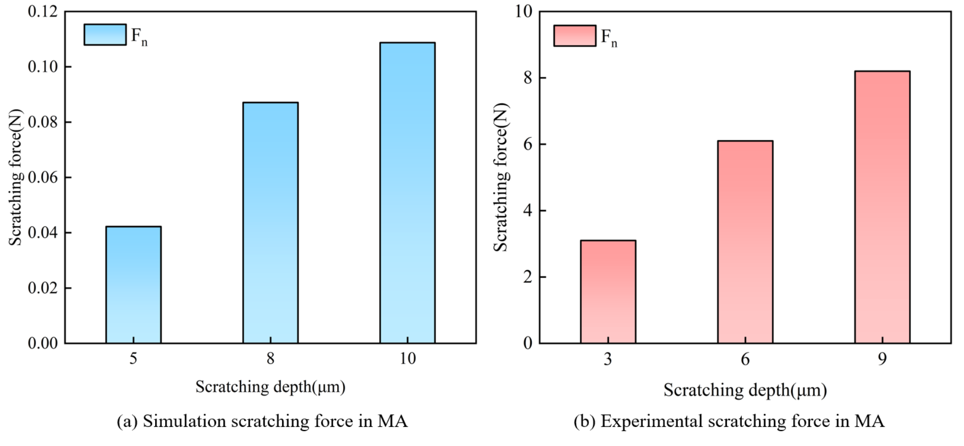

Figure 5. Simulation and experimental scratching force in MA

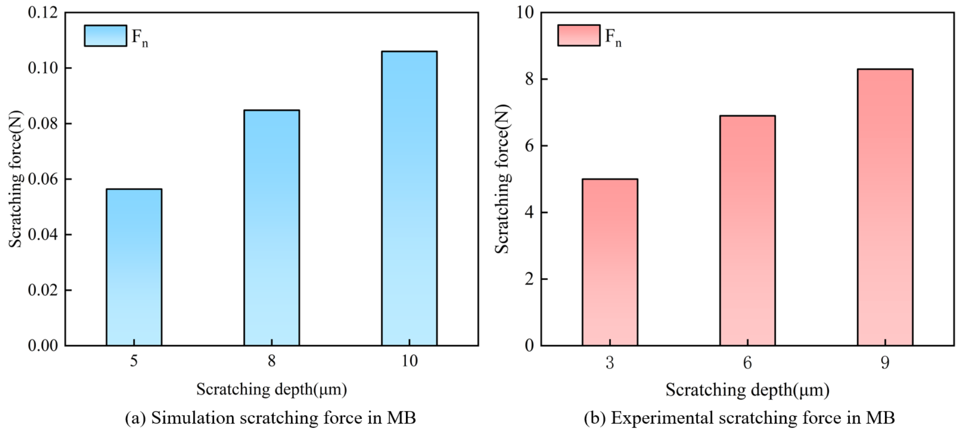

Figure 6. Simulation and experimental scratching force in MB

Figure 7 illustrates the interfacial damage between fibers and the matrix under both orientations. For MA (transverse direction), interfacial failure is effectively suppressed. In contrast, for MB (longitudinal direction), excessive stress generated after the tool advances a certain distance causes interfacial failure, inducing fiber displacement and creating pits in adjacent fibers due to localized stress concentrations. Consequently, the scratching force in the longitudinal direction (MB) is significantly larger than in the transverse direction (MA), consistent with the observed trend MB > MA.

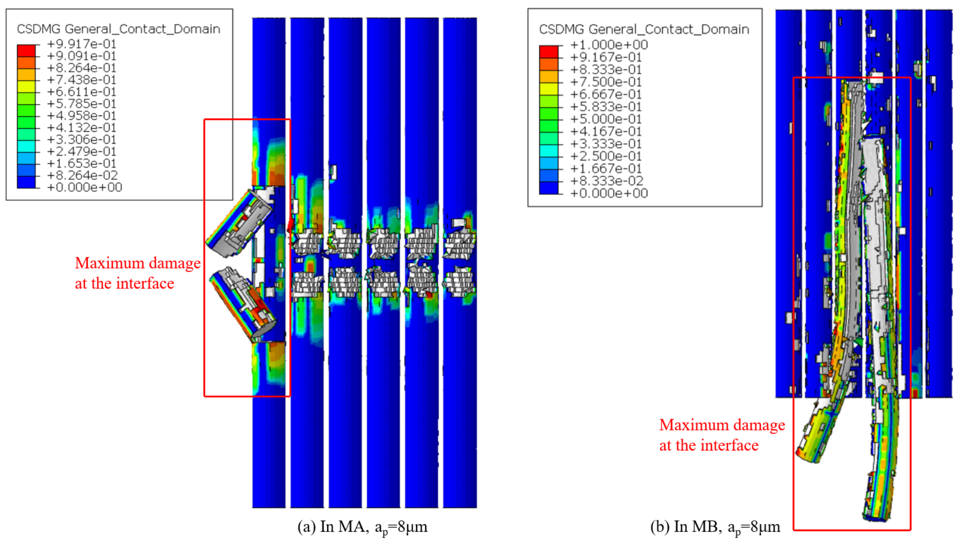

Figure 7. Simulation of fiber debonding diagram

3.2. Surface Morphology Analysis of Different Machining Directions

As shown in Figure 8, since SiC is a brittle material, it undergoes spalling when the tool passes through. With increasing scratching depth, surface crack propagation in SiC intensifies. Due to the reinforcing effect of fibers, crack extension aligns with the fiber orientation. At a scratching depth of 5 μm, minor spalling occurs at the inlet of SiC surface cracks, while crack size increases at the outlet. At 8 μm, the enlarged contact area between the tool and workpiece leads to SiC spalling and fiber exposure, with further growth in crack length at the outlet. At 10 μm, increased cutting force induces longer cracks at both inlet and outlet, accompanied by surface pits. Fibers primarily undergo shear fracture during scratching, as their dense arrangement restricts bending deformation. However, fibers at the outlet first experience bending due to tool impact, followed by bending fracture as the tool advances. With deeper cuts, increased contact area between the grit and fibers results in progressively longer fracture lengths.

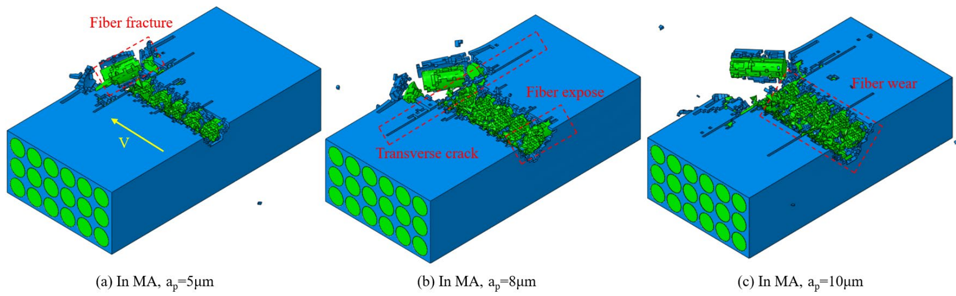

Figure 8. Simulated surface topography in MA

Figure 9 reveals that as scratching depth increases, the enlarged contact area elevates stress on the material. Once the interfacial separation stress threshold is reached, fibers are initially pulled out and undergo bending deformation. Subsequent tool advancement causes bent fibers to fracture under matrix compression. In SiC, crack fragmentation aligns with the fiber axis, and surface pits multiply. At 5 μm, fibers experience shear damage without interfacial separation; some fibers are cleanly cut along the scratching path, while minor SiC spalling exposes limited fibers. At 8 μm, shear-damaged fibers are pulled out after reaching interfacial separation stress, accompanied by fiber-matrix debonding and extensive SiC spalling, leading to significant fiber exposure. At 10 μm, reduced fiber shear damage allows direct interfacial failure. Fibers are partially pulled out, bent, and then fractured under matrix compression. Subsequent tool motion destroys residual SiC, causing fiber detachment. Widespread fiber pull-out and matrix damage further expose adjacent fibers.

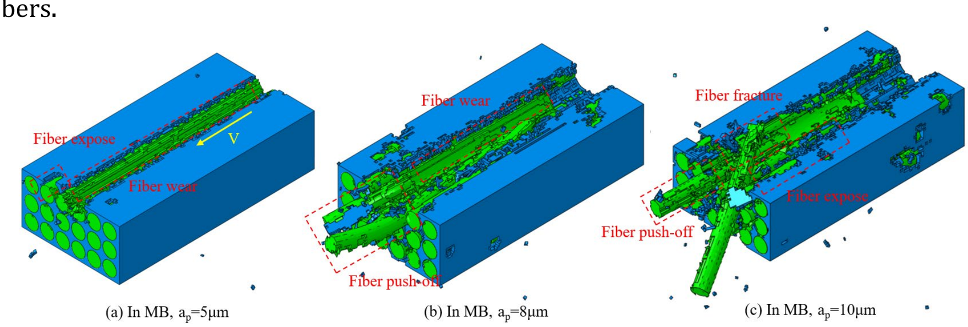

Figure 9. Simulated surface topography in MB

4. Conclusions

This study proposes a finite element numerical simulation method for Cf/SiC composites and investigates the effects of fiber orientation on grinding characteristics and removal mechanisms through single-grit scratching experiments and simulations. The following conclusions are drawn:

(1) Fiber orientation alters the mechanical behavior of fibers, influencing cutting forces and removal modes. In transverse scratching (MA), fibers predominantly fail via shear fracture, while in longitudinal scratching (MB), fibers undergo compressive failure. Transverse fibers are more easily removed compared to longitudinal fibers

(2) Periodic fluctuations in scratching forces arise from fiber arrangement patterns. The average force magnitude follows MB > MA for both orientations.

(3) Crack propagation aligns with the fiber axis. Transverse fiber removal involves wear, fracture, and peeling, with partial fiber exposure due to brittle matrix failure. Longitudinal fiber removal is dominated by wear, fracture, and pull-out, primarily governed by the contact area between fibers and the abrasive grit.

References

[1] Dai C, Yin Z, Wang P, et al (2021) Analysis on ground surface in ultrasonic face grinding of silicon carbide (SiC) ceramic with minor vibration amplitude. Ceram Int 47:21959–21968.

[2] Li F, Xiao P, Li Z, et al (2021) Microstructures and properties of C/C-SiC composites derived from different gaseous carbon matrix precursors. Ceram Int 47:30777–30789.

[3] Wei X, Cheng L-F, Zhang L-T, Xu Y-D (2006) Numerical simulation of iso-thermal chemical vapor infiltration process for fabrication of C/SiC composites. J Inorg Mater 21:1179–1184

[4] Yang C, Yang L, Xu P, et al (2024) Mechanical and microstructure characteri-sation of 2.5D C/C-SiC composites applied for the brake disc of high-speed train. Alex Eng J 108:445–458.

[5] Li L (2019) Damage development and lifetime prediction of fiber-reinforced ceramic-matrix composites subjected to cyclic loading at 1300 °C in vacuum, in-ert and oxidative atmospheres. Aerosp Sci Technol 86:613–629.

[6] Aamir M, Tolouei-Rad M, Giasin K, Nosrati A (2019) Recent advances in drilling of carbon fiber-reinforced polymers for aerospace applications: a review. Int J Adv Manuf Technol 105:2289–2308.

[7] Abidin NMZ, Sultan MTH, Hua LS, et al (2019) A brief review of computation-al analysis and experimental models of composite materials for aerospace appli-cations. J Reinf Plast Compos 38:1031–1039.

[8] Guo Y, Chen B, Fu X, et al (2024) Experimental study on grinding 2.5D C/SiC composites by electroplated grinding wheel with ordered abrasive clusters. Diam Relat Mat 142:110838.

[9] Zhang C, Chen T, Duan Z, Liu F (2024) Investigation on ultrasonic-assisted grinding of characteristics of C/SiC composites by brazed and electroplated dia-mond wheels. Int J Adv Manuf Technol 132:2171–2186.

[10] Zhang L, Ren C, Ji C, et al (2016) Effect of fiber orientations on surface grinding process of unidirectional C/SiC composites. Applied Surface Science 366:424–431.

[11] Li Y, Ge X, Wang H, et al (2019) Study of material removal mechanisms in grinding of C/SiC composites via single-abrasive scratch tests. Ceram Int 45:4729–4738.

[12] Qu S, Gong Y, Yang Y, et al (2019) Grinding characteristics and removal mechanism of

2.5D-needled Cf/SiC composites. Ceram Int 45:21608–21617.

[13] Cao X, Lin B, Zhang X (2015) Investigations on grinding process of woven ceramic matrix composite based on reinforced fiber orientations. Composites Part B: Engineering 71:184–192.

[14] Liu Q, Huang G, Cui C, et al (2019) Investigation of grinding mechanism of a 2D Cf/C-SiC composite by single-grain scratching. Ceram Int 45:13422–13430.

[15] Wang Q, Wen J, Wu C, et al (2024) Single diamond grit scratching of unidi-rectional Cf/SiC composite: Mechanical responses and fracture mechanism. Proc Inst Mech Eng Part B-J Eng Manuf 238:669–681.

[16] Lin H, Zhou M (2024) Fracture mechanism of ultrasound-assisted scratching 2D-SiCf/SiC composite fibers with different fiber orientations. J Mater Res Tech-nol-JMRT 30:9048–9060.

[17] Wu J, Song X, Gong Y, et al (2021) Analysis of the heat conduction mecha-nism for Al2O3/Silicone rubber composite material with FEM based on experi-ment observations. Compos Sci Technol 210:108809.

[18] Jia Q, Wang Y, Zhang X, et al (2022) Failure mechanism of continuous fi-ber-reinforced titanium matrix composite bling under rotational loading. J Mater Res Technol-JMRT 18:788–799.

[19] Zhu H, Feng Y, Zhou Z, et al (2024) Simulation and experimental research on longitudinal-torsional ultrasonic vibration drilling of CFRP/Ti laminates. Proc Inst Mech Eng Part B-J Eng Manuf.

[20] Du Y, Lu M, Lin J, et al (2024) Experimental and simulation research on re-moval mechanism of precision machining SiCp/Al composites based on mul-ti-phase simulation model. Alex Eng J 109:482–496.

[21] Yan X, Reiner J, Bacca M, et al (2019) A study of energy dissipating mecha-nisms in orthogonal cutting of UD-CFRP composites. Compos Struct 220:460–472.

[22] Han L, Zhang J, Liu Y, Sun T (2021) Effect of fiber orientation on depth sensing intra-laminar failure of unidirectional CFRP under nano-scratching. Compos Pt B-Eng 224:109211.

[23] Chen G, Xu J, Wang J, et al (2022) Numerical and experimental study on the amplitude effect of ultrasonic vibration-assisted milling of 3D needle-punched Cf/SiC composite. Ceram Int 48:17893–17914.

[24] Gu X, Wang H, Zhao Q, et al (2018) Effect of cutting tool geometries on the ductile-brittle transition of monocrystalline sapphire. Int J Mech Sci 148:565–577.

[25] Fouquet S, Rollin M, Pailler R, Bourrat X (2008) Tribological behaviour of composites made of carbon fibres and ceramic matrix in the Si-C system. Wear 264:850–856.

[26] Paul R, Gouda K, Bhowmik S (2021) Effect of Different Constraint on Tribo-logical Behaviour of Natural Fibre/Filler Reinforced Polymeric Composites: a Review. Silicon 13:2785–2807.